# Digital halftoning of medical images

**Ronald W. Silkman**

**Kodak Health Imaging Systems, 1669 Lake Avenue, Rochester, NY 14650-2123**

**Kevin J. Parker**

**Department of Electrical Engineering, College of Engineering and Applied Science**
**University of Rochester, Rochester, New York, 14627**

## ABSTRACT

This work considers the use of digital halftones in the display of medical images. One might assume that the use of halftone rendering (as opposed to continuous tone image rendering) will degrade the information in medical images, therefore, it is interesting to study what degree of degradation is unacceptable in medical images. We analyze various halftoning techniques quantitatively by first generating low-contrast detail diagrams (CDD) made to represent computed tomography (CT), magnetic resonance (MR), and ultrasound (US) modality images. These are then halftoned and printed using error diffusion, Bayer's method, blue noise mask, and centered weighted dots. The contrast areas in the diagram are randomly placed on a 5 x 5 grid. A single observer is used to determine the minimum contrast "lesion" that could be observed. The results for minimum detectable contrast depend on resolution (dots per inch), modality, and halftoning technique. It is shown that acceptable halftone rendering, with small degradation, can be achieved under certain conditions.

**Keywords:** Halftoning, error diffusion, Bayer's method, blue noise mask, centered weighted dots, contrast detail diagram, magnetic resonance, computed tomography, ultrasound, modality filters.

## 1. INTRODUCTION

Contrast resolution in medical images is of primary importance, because much of the detection of abnormal lesions and tissues involves the identification of low-contrast regions against a background. When generating medical images via a binary printing mechanism, the contrast resolution may be affected. This study is done to ascertain the impact of halftoning medical images produced from three major modalities,[1-3] computed tomography (CT), magnetic resonance imaging (MR), and ultrasound (US). These three imaging modalities comprise a large portion of computer generated images presently in use. Each modality has its own power spectrum caused by the different physics of each modality. The halftoning algorithms selected are Floyd-Steinberg

0-8194-1779-3/95/$6.00

error diffusion,[4] Bayer's method,[4] blue noise mask,[5] and center weighted dot.[4] Image halftoning is a nonlinear operation and therefore, is highly dependent on the spectral power of the image, the halftoning algorithm applied, and the dot size. In this study we quantify the effect of halftoning on contrast resolution of the selected modalities. This study is implemented using computer generated images that mimic the three selected modalities. The images are read by a single observer, and the size of the minimally detectable low contrast lesions are recorded.

## 2. IMAGE SET GENERATION

Figure 1 describes the process flow involved to produce the test image set. Stages 8 and 9 are the final computer generated image test set of eight films. Each film sheet, of the set of eight, was an image comprising four smaller images (subimages). The upper left subimage on a film sheet image is halftoned using error diffusion. The upper right subimage is halftoned using Bayer's method. The lower left subimage is halftoned using blue noise mask. The lower right subimage was fashioned using center weighted dot. Stage 8 comprises test images halftoned with 80 micron dots, and stage 9 comprises images halftoned using 40 micron dots.

Stages 10 and 11 are noiseless analog reference images. Each subimage is the same. These images comprise the control image set. They were produced in 8-bit analog form. Stage 10 comprises the reference images produced from a 80 micron pixel, and stage 11 are reference images produced via a 40 micron pixel.

Columns 2, 3, and 4 are images that mimic the three selected modalities of CT, MR, and US, respectively. For example, images in stages 8, 9, 10, and 11 that are in column 4, look like images produced via a US modality. Column 1 are images that were halftoned but were not passed through a modality filter. These images had +/-10% rms multiplicative noise applied to the image before halftoning.

The FIRE 240 printer is used to produce the images. The film printer used KODAK Ektascan HN film. The film is in role form 9 inches by 175 feet. The spot size of the Gaussian beam used on the FIRE is 20 υm at the half power points. The FIRE will pixel replicate an image pixel in the x and y direction one time. The final spot size is 40 υm. The result is a 40 υm square pixel that is good for halftone images.

**Figure 1. Image set generation**

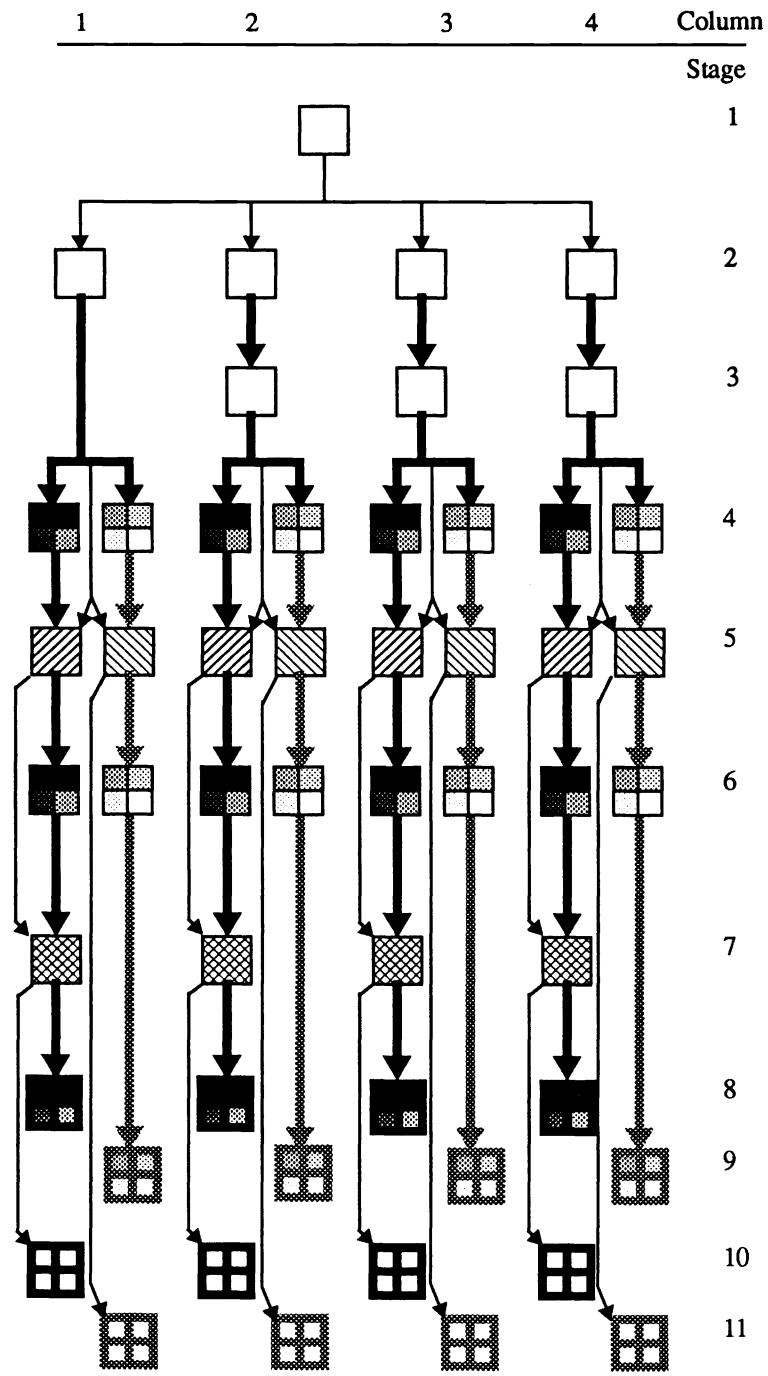

### 2.1 Reference image generation (cdi[x, y])

Rows 1-7 describe the process used to produce the test images. A single-contrast detail diagram (CDD)[6-8] was used as the source image, Fig. 1 row 1. This image is familiar to doctors as well as engineers. Equation (1) is used to computer generate the CDD and Eq. (2) is used to place noise in the image. Figure 2 shows an example of the CDD image. This single reference image then had the circular lesions randomly placed in the image but still on the same grid. Each Fig. 1 column used the same CDD image and generated four randomized reference images from it. This yields 16 images with lesions randomly placed with the same contrast and noise profile. The same random placement for row 8 is used for row 9. The observer was unaware of this, since the set of 16 for the 80-micron dot images is shown in random order with the set of 16, 40-micron dot images.

$$\mathrm{cdi}[x, y] = \frac{255}{100}\left\{\mathrm{bg}\% + \sum_{r=0}^{R-1}(D\%_r - \mathrm{bg}\%)\sum_{c=0}^{C-1} u\left(0.5 - \frac{2.0\sqrt{(x - Ox_c)^2 + (y - Oy_r)^2}}{S_c}\right)\right\} \quad (1)$$

Where bg% is the background density: (43) percent (1.65) density. $D\%_r$ is the set of circle row density: (60, 50.29, 46.31, 44.52, 43.70) percent, (1.22, 1.46, 1.57, 1.61, 1.64) density. $Ox_c$, $Oy_r$ is the set of circle column and row offsets: (85, 171, 256, 341, 427) pixels. $S_c$ is the set of column circle sizes: (64, 32, 16, 8, 4) pixels, (10, 5, 2.5, 1.25, 0.625) mm. R and C are both 5 rows and columns. x, y range from 0 to 511 pixels. One pixel is 0.15625 mm.

Independent, multiplicative white noise is scaled with the image using Eq. (2). For this study, noise level is 30 percent.[9] cdin[x, y] is contrast detail image with noise.

$$\mathrm{cdin}[x, y] = \mathrm{cdi}[x, y]\,(1 + (\mathrm{random}(1) - 0.5)\,(\frac{\text{noise level}}{100})) \quad (2)$$

**Figure 2. Basic contrast detail image (cdi[x, y]) without random lesion placement**

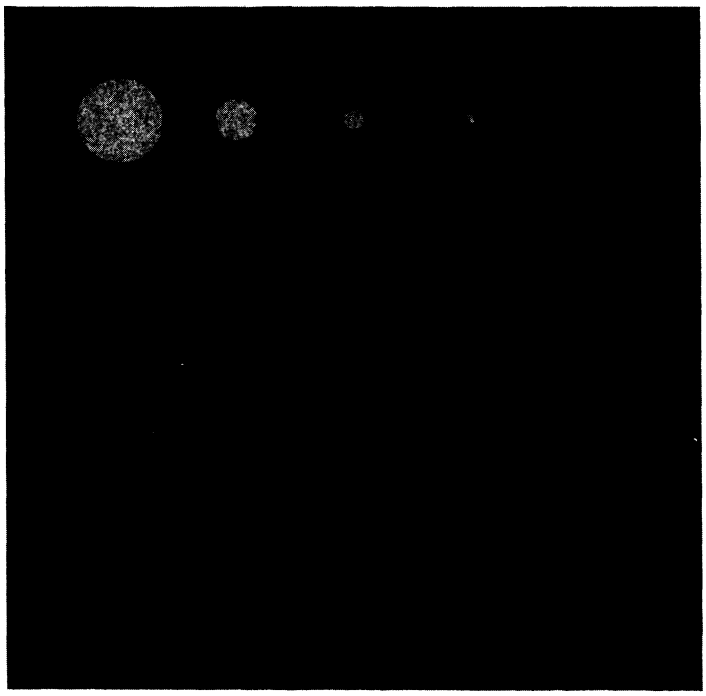

At stage 3, the 16 random images in 4 groups are passed through the modality-mimicking filters. Now the four sets are different in that each column will have a distinct resemblance to a specific imaging modality. Column 1 is the control and is unaffected. Columns 2, 3, and 4 will resemble modalities of CT, MR, and US, respectively.

### 2.2 Computed tomography-mimicking image (cti[x, y])

Figure 3 describes the flow used to produce the CT-mimicking image. Equation (3) describes the filter used to mimic the low-pass filter effects of finite CT beam width and sensor size.[2] It is a circular symmetric filter, where the profile is equivalent to a blackman filter,[10] Eq. (4). The blackman filter was used because it had the least side lobe energy of the simple circular symmetric filters and a well-defined low-pass band. x and y sample points are converted to a real valued radius in Eq. (5). This radius value per x, y samples scaled by a blackman width of 8 pixels or 1.28 mm, generates the circular filter. Figure 4 is the impulse response of bwi[x, y]. The denominator amplitude scales the filter to an area of one.[11] cti[x, y] is the final CT modality image, Fig. 5.

**Figure 3. Flow diagram for CT-mimicking image**

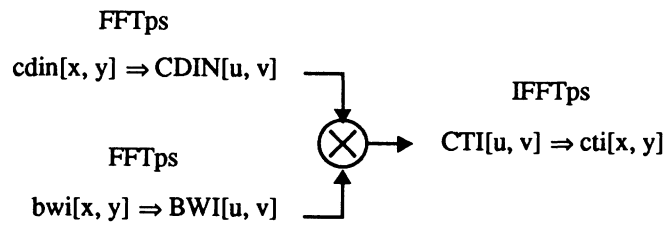


$$bwi[x, y] = \frac{black\left(\frac{2.0\ Radius(x, y)}{blackman\ width}\right)}{\sum_{y=0}^{Y-1}\sum_{x=0}^{X-1} black\left(\frac{2.0\ Radius(x, y)}{blackman\ width}\right)}$$

$$black\ (p) = (0.5 - p)\ [0.42 - 0.5\cos(2\pi(p + 0.5)) + 0.08\cos(2\pi(p + 0.5))]$$

$$Radius(x, y) = \sqrt{\left(x - \frac{512}{2}\right)^2 + \left(y - \frac{512}{2}\right)^2}$$

**Figure 4. Blackman filter impulse response**

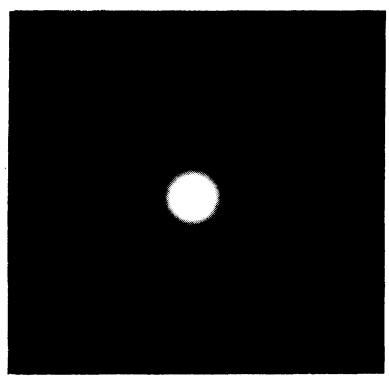

**Figure 5. CT-mimicking image**

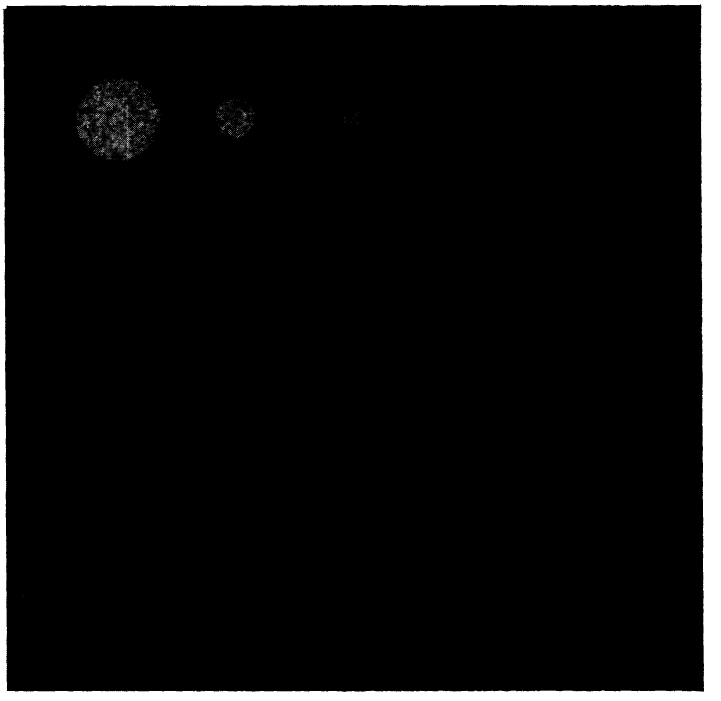

### 2.3 Magnetic resonance mimicking image mri[x, y]

Figure 6 describes the flow used to generate the MR-mimicking image mri[x, y]. The 2-D blackman filter used for the CT image is used to limit the frequency content of the source image. MR images are frequently characterized by nonsymmetric data due to time constraints in the phase encoding direction.[2,3] This nonsymmetry is modeled by vertical clipping in the frequency domain with a vertical rectangle function, Fig. 6. This rectangle function will zero any value greater than +/-70 in the vertical frequency domain axis. This action causes vertical ghosting in the image. Figure 7 depicts the MR-mimicking filter impulse response,[12,13] giving a resolution of roughly 8 pixels, 1.25 mm in the horizontal dimension, similar to that of the CT-mimcking image. mri[x, y] is the final output image and is shown in Fig. 8.

**Figure 6. Flow diagram for MR-mimicking image**

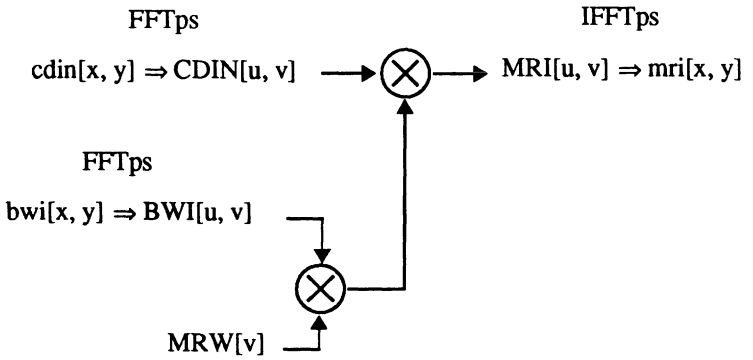


$$MRW\,[v] = u\,[70 - v] + u\,[v - (V - 70)] \tag{6}$$

**Figure 7. MR filter impulse response, showing "ghosting" in the phase encoding direction**

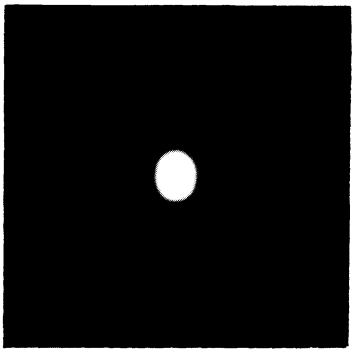

**Figure 8. MR-mimicking image**

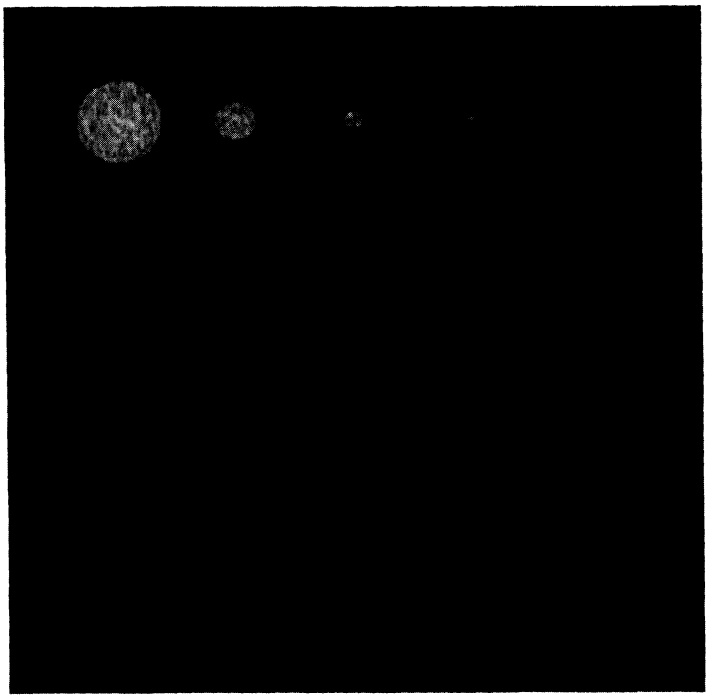

### 2.4 Ultrasound-mimicking image (usi[x, y])

Figure 9 depicts the flow to produce an US-mimicking image usi[x, y]. The US image is much more involved to construct. The input image of cdin[x, y] is converted to multiplicative zero-mean white noise[2,3] and is then rescaled to fit the 8-bit image depth, Eq. (7). This produces the intermediate image cdion[x, y]. This image is convolved with the ultrasound pulse, Eq. (8). The impulse response is shown in Fig. 10. The pulse is a 2-D Gaussian damped horizontal cosine wave having a resolution of approximately 8 pixels, 1.25 mm, roughly similar to the resolution of the CT and MR-mimcking images. After the convolution, the image is absolute valued and filtered with a 2-D blackman filter with blackman width of 16 pixels or 2.56 mm, to rectify, or find, the envelope of the signal.[14] Zero-mean filtered noise is then added to emulate electronic noise. This process yields usi[x, y], Fig. 11.

**Figure 9. Flow diagram for US-mimicking image**

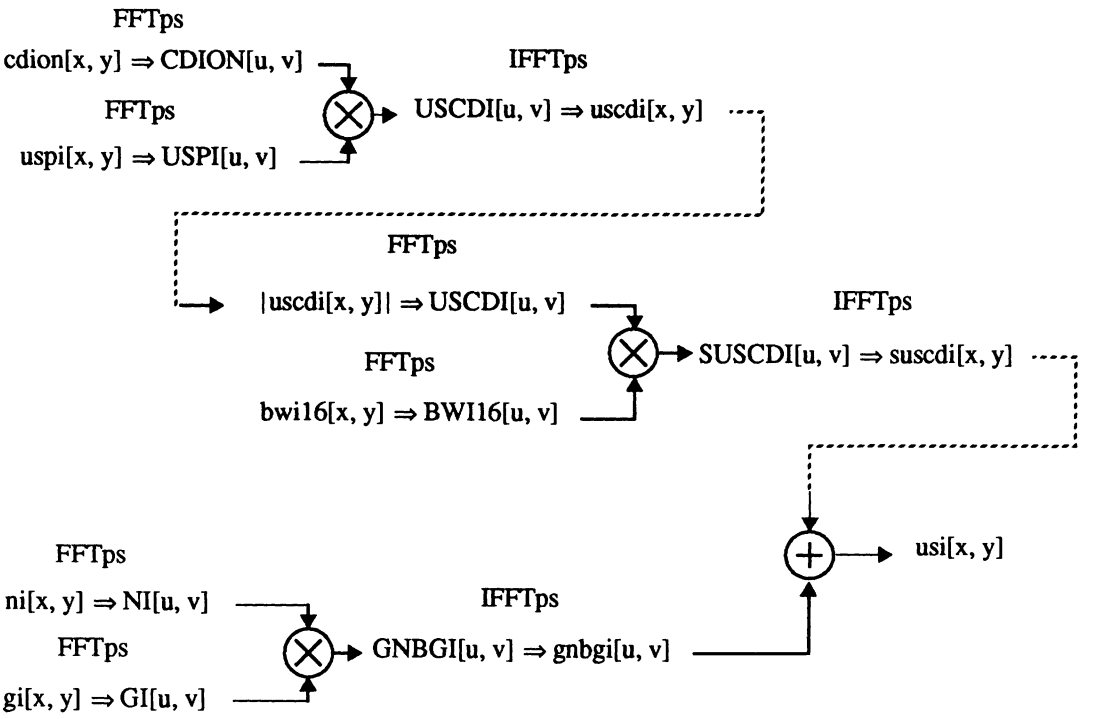


$$\text{cdion}[x, y] = 33.99\,(\text{cdi}[x, y] - \text{bg}\%\,\frac{255}{100})\,(\text{random}\,(2) - 1.0) \tag{7}$$

$$\text{uspi}[x, y] = \frac{\text{Gauss}\,(\frac{\text{Radius}(x, y)}{3.0})\,\cos\left(\frac{2\pi\,(x - \frac{512}{2})}{3.0}\right)}{\sum_{y=0}^{511}\sum_{x=0}^{511}\text{Gauss}\,(\frac{\text{Radius}(x, y)}{3.0})} \tag{8}$$

**Figure 10. Ultrasound impulse response**

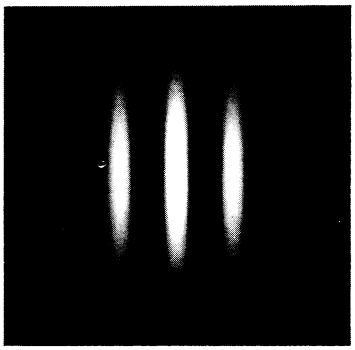

**Figure 11. Ultrasound mimicking image**

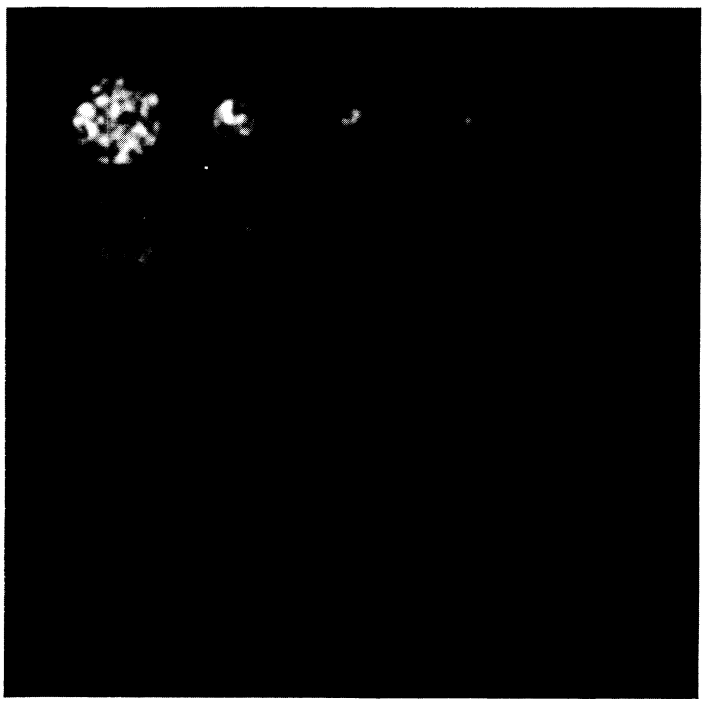

### 2.5 Histogram warping and image size scaling

The CT, MR, US-mimicking images were all produced in the computer. Stage 4 of Fig. 1 shows a histogram warping process. Each image once halftoned effects the starting densities. The density change is a function of the halftoning dot size and the halftoning algorithm. The warping alters the densities of the input images, such that the halftoned images will produce the densities originally selected. This warping is accomplished via a lookup table. There are now 32 separate images. These images

are the subimages used in stages 8 and 9 once halftoned. The black arrows depict image modality sets that will be halftoned with 80 micron dots. The grey arrows depict 40-micron dot halftoning flow. The single arrow bypassing stage 4 is the analog reference image for that modality.

Stage 5 bilinear interpolates the images up from 512 x 512 to 1024 x 1024 for the 80 micron image set and up to 2048 x 2048 for the 40-micron image set. Bilinear interpolating is used to reduce image tiling, and bicubic spline is not used due to induced rippling around lesion edges. The reference images are also scaled at this step by respective amounts.

Stage 6 is the halftoning step. The 80 and 40-micron images are halftoned using an error diffusion algorithm Fig. 12 and a thresholding algorithm is used for Bayer's method, blue noise mask, and center weighted dot.

**Figure 12. Error diffusion block diagram**

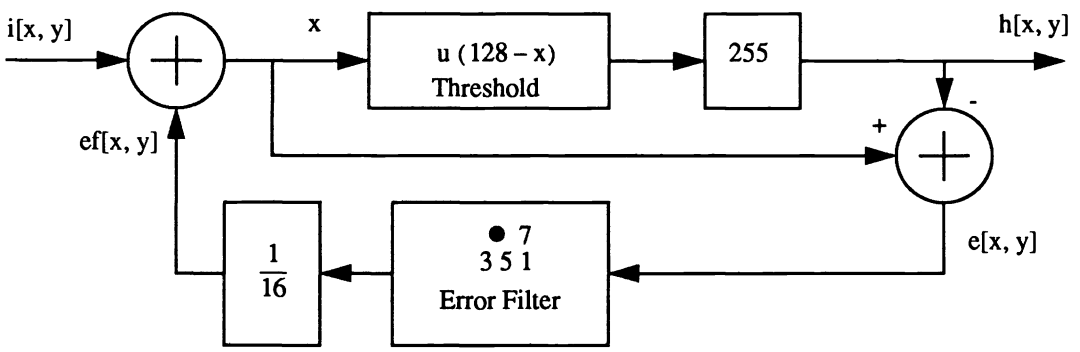


Error diffusion is a thresholding process combined with a feedback error filter. The error filter uses the quantized error and generates a feedback signal that locally places the error back into the halftoned image. In the presence of flat fields or constant i[x, y] values, error diffusion will generate a unique noise pattern with mean equal to the input image value. The algorithm works in 8-bit space, therefore, it can generate 256 different levels or densities.

**Table 1. Bayer's method threshold font matrix**

| | | | | | | | |
|---|---|---|---|---|---|---|---|
| 000 | 128 | 032 | 160 | 008 | 136 | 040 | 168 |
| 192 | 064 | 224 | 096 | 200 | 072 | 232 | 104 |
| 048 | 176 | 016 | 144 | 056 | 184 | 024 | 152 |
| 240 | 112 | 208 | 080 | 248 | 120 | 216 | 088 |
| 008 | 136 | 040 | 168 | 000 | 128 | 032 | 160 |
| 200 | 072 | 232 | 104 | 192 | 064 | 224 | 096 |
| 056 | 184 | 024 | 152 | 048 | 176 | 016 | 144 |
| 248 | 120 | 216 | 088 | 240 | 112 | 208 | 080 |

Bayer's method is a fixed grid threshold halftone algorithm. This grid, Table 1, simply tiles across the image and if the pixel under a grid value is greater than the value, a high value is placed in the halftoned image at that location, a zero is placed otherwise. This matrix has 32 patterns or densities. Blue noise mask, Table 2, and center weighted dot, Table 3, also are used in this way. They differ in the grid size, the threshold values in the grid, and/or the position of the grid value.

**Table 2. Blue noise mask partial threshold font matrix, 256 x 256**

| | | | | | | | | |
|---|---|---|---|---|---|---|---|---|
| 161 | 38 | 198 | 7 | 167 | 101 | 238 | 22 | ... |
| 122 | 92 | 66 | 223 | 121 | 69 | 35 | 227 | ... |
| 146 | 236 | 130 | 122 | 41 | 211 | 155 | 140 | ... |
| 91 | 39 | 192 | 9 | 244 | 79 | 195 | 11 | ... |
| 199 | 107 | 220 | 83 | 180 | 25 | 124 | 152 | ... |
| 53 | 162 | 19 | 204 | 69 | 225 | 42 | 117 | ... |
| 89 | 244 | 109 | 46 | 150 | 114 | 68 | 248 | ... |
| 167 | 26 | 79 | 187 | 235 | 25 | 190 | 100 | ... |
| ... | ... | ... | ... | ... | ... | ... | ... | ... |

Blue noise mask matrix is 256 x 256 pixels in size. Table 2 shows the upper left 8 x 8 section as an example. This grid is precisely generated, such that when the image is halftoned, the dots form an image and the dots are separated at some known distance with a known variance. The two flagged numbers show that this matrix has 256 patterns or densities.

**Table 3. Center weighted dots threshold font matrix.**

| | | | | | | | |
|---|---|---|---|---|---|---|---|
| 112 | 096 | 104 | 128 | 152 | 168 | 160 | 136 |
| 040 | 032 | 024 | 080 | 224 | 232 | 240 | 184 |
| 048 | 008 | 016 | 088 | 216 | 000 | 248 | 176 |
| 072 | 056 | 064 | 120 | 192 | 208 | 200 | 144 |
| 152 | 168 | 160 | 136 | 112 | 096 | 104 | 128 |
| 224 | 232 | 240 | 184 | 040 | 032 | 024 | 080 |
| 216 | 000 | 248 | 176 | 048 | 008 | 016 | 088 |
| 192 | 208 | 200 | 144 | 072 | 056 | 064 | 120 |

Center weighted dot is an 8 x 8 thresholding matrix. The matrix simply grows 2 dots at 45 degrees as the density in the image increases. The matrix has only 32 patterns or densities levels.

Row 7 is a further up scaling for the 80-micron images. This scaling is a 2 x 2 pixel replication. This is used to scale the halftone dots up to 80 micron. The 80-micron reference images were also pixel replicated by 2 x 2.

## 3. VISUAL ANALYSIS

A single person observer expert in medical imaging science was used to analyze the computer-generated halftoned modality images. He was asked to denote image regions, with some confidence, where a lesion was present. The transparency images were all viewed on a standard X-ray luminator at a level 2 lumination. The viewing distance was 15 to 17 inches. The images were randomly selected. The reference images were viewed as a separate group two weeks later and also randomly selected. Scores were kept of all true positive and false negatives. We did not evaluate for the statistics of false positives, although these did occur occasionally.

## 4. RESULTS AND CONCLUSIONS

We summarize the results in two tables and three graphs. Table 4 shows the halftone algorithm that will render the best contrast rendition within a factor of 2, compared to the reference image set of contone images. Table 5 shows which artifacts are predominant in the image sets.

**Table 4. 40 micron acceptable methods**

| Modality | Reference graph | Halftone algorithm |
|---|---|---|
| CT | graph 1 | CENT |
| MR | graph 2 | BAY, BLUE, CENT |
| US | graph 3 | BLUE, CENT |

Graphs 1, 2, and 3 show the minimum detectable contrast for CT, MR, and US, respectively. "Error, bay, blue, and cent" implies "error diffusion, Bayer's method, blue noise mask, and centered weighted dot" halftoning processes. "Ref" implies a modality altered image that is not halftoned. This is the comparison level within a modality and across modalities. The x axis is the object diameter size in pixels, where 1 pixel is 0.15625 mm. The y axis is the object (lesion) contrast. The lines are a linear regression through the data points. The graphs are on log-log scale. Small low contrast objects are near the lower left in the graphs and large bright objects are near the upper right part of the graphs. The lower a linear regression line is in the graph, the better contrast resolution is for that halftone process and modality in that local size and contrast range. The more horizontal a line is, the better the overall contrast resolution for a halftoning process with a specific modality. If a halftoning line is below the reference line, some aspect of the halftoning process is accentuating the local contrast in the image, be it contrast quantizing and/or texture changes.

The "ref" line in each graph is a measure of how the mimicking algorithm effected the contrast resolution. In graph 2, the "ref" line is high in the small diameter object area. This implies that the modality has low-spacial frequency response. This could be said of MR compared to the "ref" line in graph 1, which is a CT modality. This modality has only one filter effecting the image, where MR has 2 filters effecting the image. Graph 3 is ultrasound modality. The "ref" line here also depicts a better small diameter contrast resolution. Here, the reason is more likely that the algorithm is causing the size of the objects to increase due to the Gaussian damped cosine pulse.

For graph 1, Bayer's method and centered weighted dot showed better contrast resolution than the "ref" line for large objects around 64 pixels. These two halftoning processes had the least threshold matrix size. Here, contrast quantizing and/or low frequency texture changes help the observer to realize low contrast objects. In all, centered weighted dot displayed the best contrast resolution relative to the "ref" line, with some enhancement with large object sizes.

In graph 2, Bayer's method displayed a better than "ref" line consistently for all object sizes. Center weighted dot and blue noise mask both show good contrast resolution compared to the "ref" line. For objects below 20 pixels, blue noise mask and centered weighted dot have good relative contrast resolution. Above 20 pixels, Bayer's method yields better contrast with some enhancement due to textural changes.

In graph 3, blue noise mask and centered weighted dot share best relative contrast resolution. Larger than 10 pixel object sizes are rendered best by blue noise mask, where below that limit centered weighted dot halftoning process is best.

Error diffusion in all graphs had least relative contrast resolution. In the presence of image noise, error diffusion generates more noise. This tends to break up edges on low contrast objects and obscure small objects.

**Table 5. Artifacts generated per halftone process**

| Halftone rendering | Artifacts |
|---|---|
| Error diffusion | worming, false positives |
| Bayer's method | quantization, periodicity |
| Blue noise mask | low-spatial frequency noise |
| Center weighted dots | quantization, periodicity |

None of the halftoning algorithms produced at this time, with the dots per inch available of 600, could fully duplicate or surpass the level of analog printing used today. Future studies are required to evaluate higher resolution printers and improved halftone methods.[15] Comprehensive details of this study are found in the source MS thesis.[16]

**Graph 1**

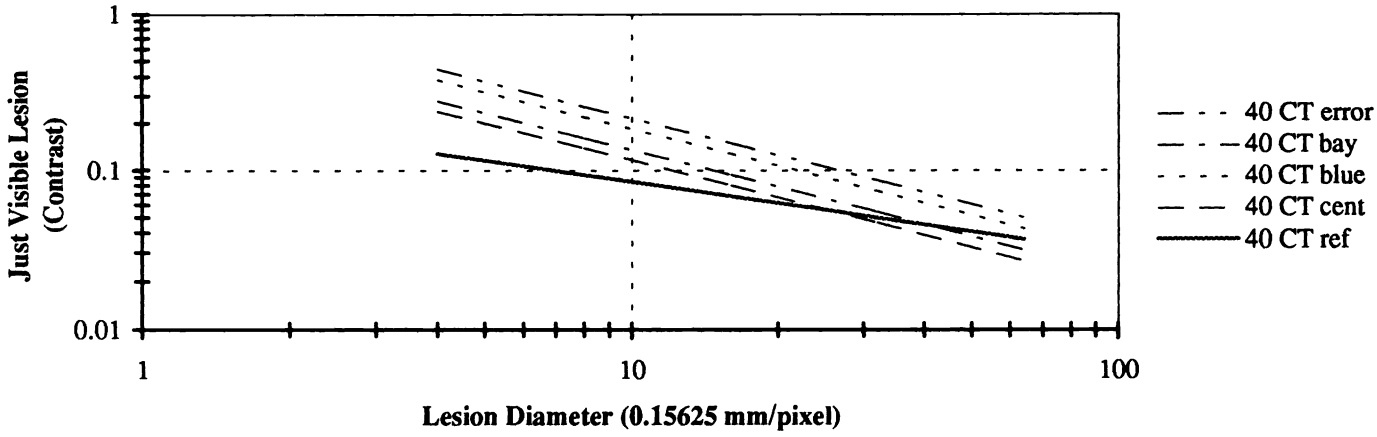


**Graph 2**

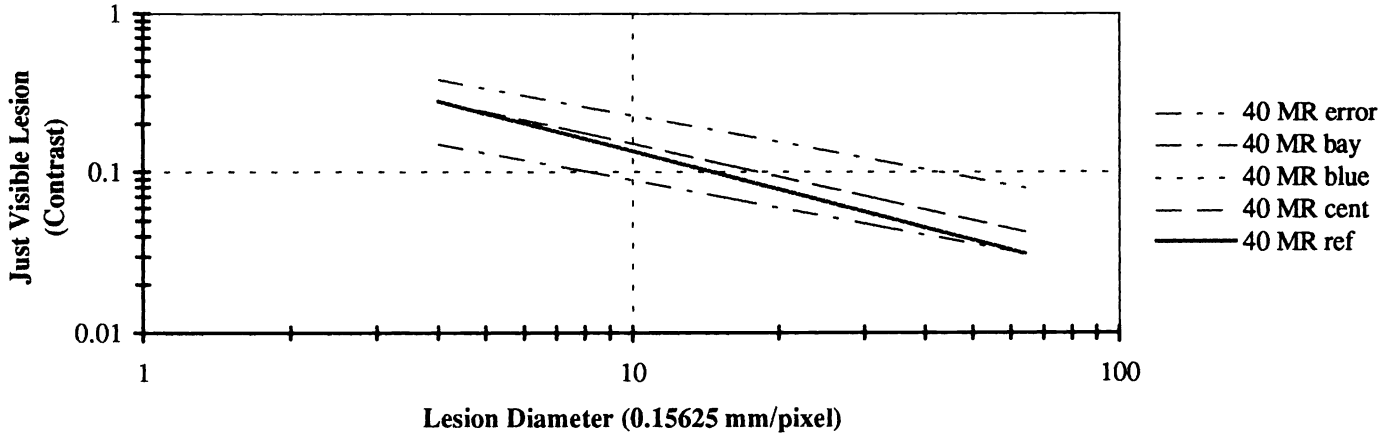


**Graph 3**

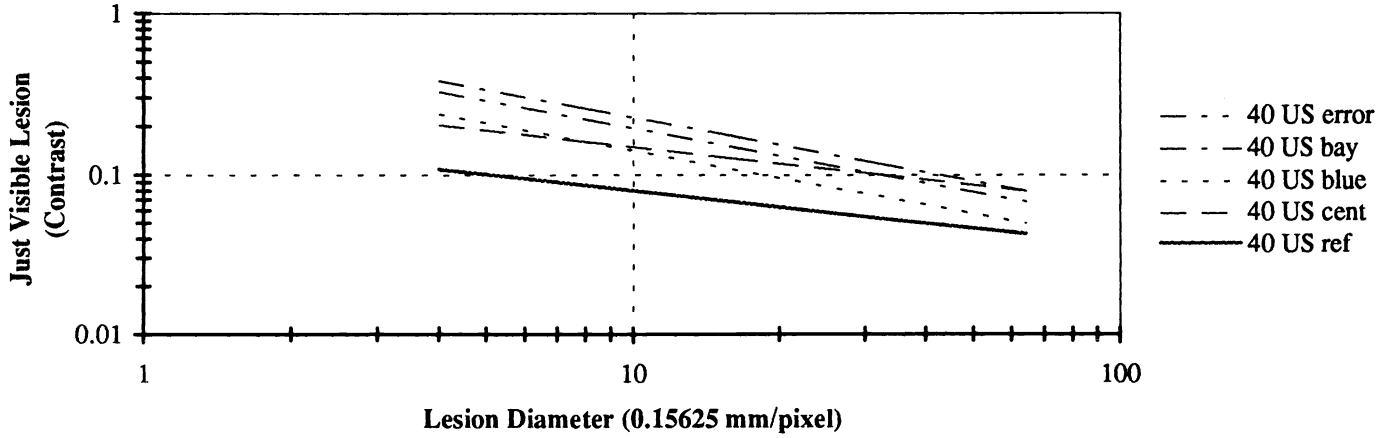

## 5. ACKNOWLEDGMENTS

I wish to thank Dr. Kevin J. Parker, Dr. Bruce Whiting, Dr. Rick Lubinsky, Dr. Cao Chi, Dr. John F. Hamilton, Jr., and Dick Blazey for allowing me this opportunity to do masters research with the University of Rochester. This experience of working with such a diversified group of university and industrial sector personnel has given me a greater appreciation of the needs of both worlds.

## 6. REFERENCES

[1] Charles E. Swenberg and James J. Conklin, Imaging Techniques in Biology and Medicine, Academic Press, Inc., California, 1988.

[2] Albert Macovski, Medical Imaging Systems, Prentice-Hall, New Jersey, 1983.

[3] Harrison H. Barrett and William Swindell, Radiological Imaging Vol I,II, Academic Press, New York, 1981.

[4] Robert Ulichney, Digital Halftoning, The MIT Press, Massachusetts, 1986.

[5] T. Mitsa, KJP, "Digital Halftoning Using a Blue Noise Mask", JOSA, Vol 19 (11), pp. 1920-1929, 1992.

[6] Albert Rose, VISION: Human and Electronic, Plenum Press, New York, 1973.

[7] A. LI Evans, The evaluation of medical images, Adam Hilger Ltd, Bristol, 1981.

[8] Thomas Woodlief, Jr., Editor, SPSE Handbook of Photographic Science and Engineering, John Wiley & Sons, Inc., New York, 1973.

[9] Dr. Kevin J. Parker, University of Rochester MRI noise study, 1991.

[10] Alan V. Oppenheim and Ronald W. Schafer, Discrete-Time Signal Processing, Prentice Hall, New Jersey, 1989.

[11] J. W. Goodman, Introduction to Fourier Optics, McGraw-Hill, New York, 1968.

[12] A. V. Oppenheim, A. S. Willsky, and I. T. Young, Signals and Systems, Prentice-Hall, Inc., New Jersey, 1983.

[13] Jae S. Lim, Two-Dimensional Signal and Image Processing, Prentice-Hall, Inc., New Jersey, 1990.

[14] B. P. Lathi, Modern Digital And Analog Communications Systems, Holt, Rinehart and Winston, Inc., Florida, 1989.

[15] M. Yao, KJP, "Modified Approach to the Construction of a Blue Noise Mask", JEI, Vol 3 (1), pp. 92-97, 1994.

[16] R. W. Silkman, "Digital Halftoning of Medical Images", MS thesis, University of Rochester, Rochester, New York, 1993.